AIAA 2008-5810

12th AIAA/ISSMO Multidisciplinary Analysis and Optimization Conference
Sep. 10–12, 2008/British Columbia, Canada

Helicopter Rotor Design Using a Time-Spectral and Adjoint-Based Method

Seongim Choi [*]
Stanford University, Stanford, CA 94305

Mark Potsdam [†]
U. S. Army Aeroflightdynamics Directorate, RDECOM
Moffett field, CA 94035

Kihwan Lee [‡] Gianluca Iaccarino [§] and Juan J. Alonso [¶]
Stanford University, Stanford, CA 94305

A time-spectral and adjoint-based optimization procedure that is particularly efficient for the analysis and shape design of helicopter rotors is developed. The time-spectral method is a fast and accurate algorithm to simulate periodic, unsteady flows by transforming them to a steady-state analysis using a Fourier spectral derivative temporal operator. An accompanying steady-state adjoint formulation for periodic unsteady problems is then possible and enables an unsteady flow design optimization procedure. The time-spectral CFD analysis is validated against conventional time-accurate CFD and flight test data for a UH-60A Black Hawk helicopter rotor in high speed forward flight. A multidisciplinary structural dynamics and comprehensive analysis coupling is employed for validation study to include blade structural dynamics and to enforce vehicle trim. Application of the adjoint-based design method is carried out to optimize blade shape for a UH-60A. An uncoupled aerodynamics only calculation is performed for design application, holding the blade deformations and trim angles fixed to the previously calculated values. Minimization of power is pursued with non-linear constraints on thrust and drag force, resulting in a simplified form of the trim condition. The blade twist distribution, airfoil section shapes, and outboard planform shape comprise over 100 design variables. Starting from the initial configuration, the optimizer found a new design that shows good performance improvement, amounting to a 2% decrease in torque and 7% increase in thrust compared to the baseline UH-60A. The results demonstrate the potential of the time-spectral and adjoint-based design method for helicopter rotors.

I. INTRODUCTION

A time-spectral method is a fast and efficient algorithm based on a classical Fourier collocation method[1] that is one of the standard methods in fluid dynamics which provide spectral accuracy for partial differential equations with periodic boundary conditions.[2] It approximates the periodic solutions by a discrete Fourier expansion and applies the spectral method to a temporal discretization of the governing equations. The method is well suited for simulation of unsteady, periodic flows, which are encountered in a number of

[*]Research Associate, Department of Aeronautics and Astronautics
[†]Research Scientist
[‡]Ph.D candidate, Department of Aeronautics and Astronautics
[§]Assistant Professor, Department of Mechanical Engineering
[¶]Associate Professor, Department of Aeronautics and Astronautics

engineering problems including turbomachinery,[3,4] flapping wings, and micro air vehicles. Its application to helicopter rotor flow analysis has been carried out in our previous work,[5–7] and by other researchers using harmonic balance methods.[8–10]

The previous work has validated the time-spectral methodology on a UH-60A Black Hawk helicopter rotor for several level flight conditions - high speed (c8534), low speed (c8515/8513), and high thrust coefficient and dynamic stall (c9017). A state-of-the-art CFD/CA (Comprehensive Analysis) coupling method was also successfully tested to account for aero/structure interaction using computational structural dynamics (CSD) and a fluid-structure interface.[6,7] The capability of the time-spectral method for accurate rotor flow analysis was investigated in detail and compared against conventional time accurate analysis and Army/NASA flight test data.

One of the advantages of the spectral method is that Fourier collocation differentiation can be represented by a simple matrix form, instead of applying a Discrete Fast Fourier transform (DFFT) and inverse DFFT between time and frequency domains.[11,12] Thus, if the matrix form of the Fourier collocation differentiation is applied to the time derivative term in the governing equations, the formulation becomes periodic steady-state in the time domain, and the solution procedure becomes independent of time evolution. This fact is appreciated to a large extent in the case of turbomachinery simulations where initial transient time to reach periodic steady-state is considerable. However, helicopter rotor flows typically take less time to reach periodic steady-state convergence (1-3 rotor revolutions), depending on the flight condition.

The adjoint-based design optimization method[13,14] has been successfully employed as an efficient and accurate technique in a wide range of aerodynamic/aero-structural shape optimization problems.[15–17] The ability to leverage an adjoint solution to inexpensively obtain the sensitivity of a particular cost function with respect to a large number of design variables has motivated the use of such a tool in a variety of design applications. The method becomes significant in a gradient-based optimization procedure, since the number of design variables can be generally independent of the computational cost. Compared with finite difference gradients, it provides higher accuracy at a much reduced cost.[15] Therefore, a complex design problem, such as fixed wing, turbomachinery, or helicopter rotor optimization, which inevitably involves a large scale simulation with a large number of design variables, can greatly benefit from the adjoint-based optimization method.

However, the application of the adjoint method has been focused so far mainly on steady-state problems. Unsteady adjoint formulations require storing the entire time history of the flow solutions, which entails massive storage/memory requirements and computational costs.[18] Some efforts to ameliorate this situation have been proposed,[19–21] however, the robustness and efficiency of the truly unsteady adjoint formulation have not yet been fully investigated, and difficulties associated with implementation of the adjoint formulation for viscous, unsteady flow solvers make the problem more challenging. Therefore, until now, its direct application to helicopter rotor design has been limited as rotor flows are turbulent and unsteady.

The characteristic related to the steady-state formulation of the time-spectral method bears significant importance from a design optimization viewpoint. It enables steady adjoint formulations to be leveraged in unsteady periodic problems. Additional terms for the spectral time-derivative in the governing equations can be easily implemented into the discrete adjoint formulation, and the solution procedure is the same as for steady problems. Although increased size of the adjoint matrix resulting from an additional term for the spectral derivative makes the solution procedure more expensive in time and memory, the efficiency compared to the direct solution of the unsteady adjoint is still considerable. Combined with any type of gradient-based optimization technique, time-spectral and adjoint-based methodology has a great potential for design optimization of unsteady, periodic problems.

The main objective of the present study is to demonstrate the capability of a design tool based on the time-spectral and adjoint-based method, by applying it to the shape optimization problem of a helicopter rotor blade in unsteady, periodic forward flight. The current study is an extension of previous work[22] where hover was chosen as the test problem and only airfoil shape changes were considered. A hovering rotor can be transformed to a steady-state problem without the use of the time-spectral method. Other researchers[23] have also investigated rotor design in hover using high performance, high fidelity, state-of-the-art optimization methods. However, forward flight optimization of a three-dimensional rotor blade using high fidelity CFD methods has only recently been enabled with advances in the time-spectral CFD methodology. Previous rotor optimization methods have utilized low fidelity aerodynamics (lifting line and vortex wakes) embedded in rotorcraft comprehensive codes[24] in order to handle the highly multidisciplinary nature of the problem.

In this paper, optimization is investigated in unsteady forward flight condition. We consider planform

shape optimization including tip shape (sweep and chord), twist distribution and airfoil sectional changes along the span. A minimization of torque is pursued at constant or higher thrust level and the drag force is constrained to be below the baseline value.

Imposition of realistic constraints in forward flight is not an easy problem without a fully coupled CFD/Comprehensive analysis solution, as a trim condition must be achieved through an iterative solution procedure accounting for aerodynamic and structural dynamic interaction. It typically requires optimization process via a CFD/CSD/CA coupling method to determine a new set of control angles and aeroelastic deformations for a new design candidate at each design step. Thus, a realistic trim constraint requires multidisciplinary design methodology which incorporates structural analysis and flight dynamics of the helicopter rotor. However, our current design methodology is mostly within an aerodynamic scope, and incorporation of structural analysis coupling is not yet implemented. Thus, a certain degree of simplification of the design problem and aeroelastics is imposed. For computational efficiency, a single blade analysis is employed in our study.

This paper is organized as follows. The theoretical background and mathematical formulation of the time-spectral method and the discrete adjoint method are described in Sections II and III, respectively. Validation of the method is shown in Section IV. Time-spectral simulation of high speed flight of the UH-60A using CFD/CA coupling is compared with flight test and time-accurate results in Section IV-B-1. To show the validity of the single blade analysis used in our design, we briefly show previous results in Section IV-B-2 comparing the four-blade and single-blade analyses with and without wake coupling. Section IV-C shows the validation of the time-spectral and adjoint-based analysis tool applied to the simulation of a two-dimensional pitching airfoil, and the sensitivity of the aerodynamic force is compared with finite difference results. Section IV-D presents an application of the design method to the problems of steady hovering flight of UH-60A rotor blade as a final validation case. Finally, an application of the current design method to an unsteady, high speed forward flight case is presented in Section V. This paper finishes with conclusions and future work.

II. TIME-SPECTRAL METHOD

The main advantage of the spectral method is the high-order accuracy it achieves compared to the finite difference method. Spectral accuracy can be obtained when the number of harmonics, larger than Nyquist frequency, are included in the solution approximation. It has proven to be equivalent to the accuracy of the infinite-order finite difference method.[2] With a much smaller number of Fourier nodes (time instances), the method demonstrates higher than or eqaul accuracy to that of the finite difference mehod.

However, since the time-spectral method is based on the Fourier collocation method, it inherently contains the error behavior of the classical Fourier spectral method: truncation error and aliasing error. The accuracy of the time-spectral method is greatly dependent on the number of Fourier modes included in a solution approximation. At the same time, the time-spectral method is a global scheme requiring solutions at all grid points in time during the solution procedure. The inclusion of a larger number of time instances improves the accuracy at a spectral convergence rate, but unavoidably incurs an increase in computational expense which deteriorates the efficiency of the time-spectral method. A rigorous study on the effects of the number of time instances on accuracy, solution convergence, and computational time savings is discussed in our previous work[7] by quantifying aliasing errors in the time-spectral computation of rotor flows. A brief summary of the mathematical formulation of the time-spectral method follows.

A. Mathematical Formulation

The Navier-Stokes equations in semi-discrete form can be written as

$$V\frac{\partial u}{\partial t} + R(u) = 0, \quad u = \begin{pmatrix} \rho \\ \rho u' \\ \rho v' \\ \rho w' \\ \rho E \end{pmatrix}, \tag{1}$$

where u is the vector of conservative variables, and $R(u)$ is the residual of the spatial discretization of viscous,

inviscid, and numerical dissipation fluxes. If we approximate u by a discrete Fourier series at N integer points in time,

$$u_j^N = \sum_{k=-N/2}^{N/2-1} \tilde{u}_k e^{ikt_j} \quad (j = 0, ..., N-1), \quad t_j = \frac{T}{N} j \ , \tag{2}$$

where T is the period, and u_j^N represents the truncated Fourier series of u up to N. $\tilde{u}_k$ is a discrete Fourier coefficient of the variable u defined as,

$$\tilde{u}_k = \frac{1}{N} \sum_{j=0}^{N-1} u_j^N e^{-ikt_j} \quad k = -N/2, ..., N/2-1 \tag{3}$$

For the collocation method Equation 1 is required to be satisfied at each point,

$$\frac{\partial u_j^N}{\partial t} + R(u_j^N)|_{t=t_j}, \quad j = 0, 1, ..., N-1 \tag{4}$$

On the other hand, a differentiation of u in physical space can be obtained by the inverse transformation of the discrete Fourier coefficients multiplied by ik. Then the approximate derivative at the grid points are given by

$$\frac{\partial u_l^N}{\partial t} = (\mathcal{D}_N u)_l = \sum_{k=-N/2}^{N/2-1} a_k e^{ikt_l} \quad (l = 0, 1, ..., N-1), \quad \text{where } a_k = ik\tilde{u_k} = \frac{ik}{N} \sum_{j=0}^{N-1} u_j^N e^{-ikt_j} \tag{5}$$

Equation 5 can be reprented by a matrix form by combining two terms in Equation 5,

$$(\mathcal{D}_N u)_l = \sum_{j=0}^{N-1} (D_N)_{lj} u_j^N, \quad \text{where } (D_N)_{lj} = \frac{1}{N} \sum_{k=-N/2}^{N/2-1} ike^{ik(t_l - t_j)} \tag{6}$$

Application of the Fourier collocation derivative operator to Equation 4 leads to,

$$D_N U + R(U) = 0, \quad \text{where } U \text{ is a vector of } (u_0^N, \ u_1^N, ..., u_{N-1}^N) \tag{7}$$

If a pseudo-time derivative term is directly added for time integration, then Equation 7 can be represented as,

$$V\frac{\partial u_j^N}{\partial \tau} + V D_N u_j^N + R(u_j^N) = 0 \ (j = 0, 1, 2, ..., N-1) \ , \tag{8}$$

which is the final form of the time-spectral equation. Compared to the original Equation 1, Equation 8 has a simpler form as a steady-state formulation. A matrix form of derivative operator can be written as a closed form as below with a odd number of grid points (time instances),

$$(D_N)_{lj} = \begin{cases} \frac{1}{2}(-1)^{l+j} cosec(\frac{(l-j)\pi}{N}) & : l \neq 0 \\ 0 & : l = j \ . \end{cases} \tag{9}$$

This matrix is skew-symmetric and the corresponding eigenvalues are $ik, \ k = -(N-1)/2, .., (N-1)/2$, with an odd number N. If we have an odd number of time instances, then the zero eigenvalue has single multiplicity rather than double multiplicity in the case of an even number of time instances. We choose to have an odd number of time instances for the spectral formulation in our study for stability reasons related to the eigenvalues.[2]

III. DISCRETE ADJOINT METHOD

The design problem in our study is posed as a general form of the optimization problem of finding the minimum of the objective/cost function, I, with respect to a number of design variables, x, while satisfying a set of constraints, C. The cost function, I, is also dependent upon the state vector, u, which can be obtained by solving the governing equations, R. This design problem can be written mathematically,

$$\begin{aligned} \text{Minimize} \quad & I(x, u(x)) \\ \text{w.r.t} \quad & x \ , \\ \text{subject to} \quad & R^*(x, u(x)) = 0 \\ & C_i(x, u(x)) = 0 \ (i = 1, ..., m) \ , \end{aligned}$$

where the governing equation R^* represents the time-spectral form of the Euler or Navier-Stokes equations in Equation 8, and m additional constraints are satisfied by the equations $C_i(x, u(x))$. The sensitivities of the cost function with respect to the design variables are obtained by applying the chain rule, and a variation of I can be represented, to the first order, as

$$\delta I = \frac{\partial I^T}{\partial u}\delta u + \frac{\partial I^T}{\partial x}\delta x \tag{10}$$

Since the derivative of the cost function is dependent on both the design variables, x, and the state vector, u, a new flow solution is required for each parameter with respect to which we are seeking a derivative. As an alternative to the direct solution of Equation 10, we introduce the governing equations as a constraint using the method of Lagrange Multipliers, ψ, which makes it possible to obtain an expression for δI that is independent of δu. The gradient of I with respect to n arbitrary number of design parameters can be calculated without re-evaluating the flow equations.

In other words, since the governing equations of the time-spectral formulation of the Euler/Navier-Stokes equations are given by $R^*(x, u(x)) = 0$ and they should always be satisfied, the variation of the residual must be zero and can be derived as,

$$\delta R^* = \left[\frac{\partial R^*}{\partial u}\right]\delta u + \left[\frac{\partial R^*}{\partial x}\right]\delta x = 0 \tag{11}$$

As δR^* is identically zero, it can be added or subtracted to Equation 10 to yield,

$$\begin{aligned} \delta I &= \frac{\partial I^T}{\partial u}\delta u + \frac{\partial I^T}{\partial x}\delta x \ - \psi^T\left(\left[\frac{\partial R^*}{\partial u}\right]\delta u + \left[\frac{\partial R^*}{\partial x}\right]\delta x\right) \\ &= \left\{\frac{\partial I^T}{\partial u} - \psi^T\left[\frac{\partial R^*}{\partial u}\right]\right\}\delta u \ + \ \left\{\frac{\partial I^T}{\partial x} - \psi^T\left[\frac{\partial R^{*T}}{\partial x}\right]\right\}\delta x \end{aligned} \tag{12}$$

To remove the dependence of δI on δu, the adjoint variable, ψ can be chosen such that the first part of the right hand side of Equation 12 is zero. Thus as long as ψ satisfies the adjoint equation,

$$\left[\frac{\partial R^*}{\partial u}\right]^T \psi = \frac{\partial I}{\partial u} \ , \tag{13}$$

then the sensitivity Equation 10 becomes independent of δu,

$$\delta I = \left\{\frac{\partial I^T}{\partial x} - \psi^T\left[\frac{\partial R^*}{\partial x}\right]\right\}\delta x \tag{14}$$

The adjoint matrix $\left[\frac{\partial R^*}{\partial u}\right]$ in Equation 13 is a sparse matrix of constant coefficients (which depend on the periodic flow solution u) and can be set up by deriving or computing the dependence of the residual in one cell of the mesh on the flow solution at every cell in the domain. Since the residual evaluation has a compact stencil (mostly composed of nearest neighbors) the number of non-zero entries in each column of the matrix is small. For the current flow solver, SUmb, and for the discretization used in this work, the residual at one

point is influenced by the flow solution at 33 neighboring cells in Navier-Stokes solutions and 9 cells in Euler solutions. In addition, through the coupling of the time-spectral derivative term, the solution at a point also depends on the solution at the same point, but at all the time instances considered in the solution of the periodic problem. The influence of all other time instances on one is included in an adjoint matrix in a fully coupled manner rather than separated in the right-hand side of the adjoint equation.

The computation of all non-zero entries of the matrix and storage during the iterative convergence process requires a considerable amount of memory. Instead, we recompute these terms at every iteration of the adjoint solution, reducing the memory penalty. Furthermore, we have chosen a solution procedure that employs an ILU-preconditioned GMRES algorithm (in the form of the PETSc toolkit) that has proven to be both efficient and robust in the solution of the relatively small problems treated in this work. For larger problems, the convergence rates of this solution approach deteriorate, but the additional multigrid as a preconditioner for the GMRES iteration is able to restore the convergence rates to more reasonable values.

The solution of the sensitivity Equation 14 becomes straightforward to obtain, as $\frac{\partial I}{\partial x}$ and $\frac{\partial R^*}{\partial x}$ are easily computed. Once we know the objective function values and the gradient information with respect to the design variables, any gradient-based optimization algorithm can be applied to locate the optimum value of the objective function.

IV. VALIDATION OF AERODYNAMIC ANALYSIS TOOLS

The accuracy of the analysis tools in a design procedure is crucial in proving credibility of the optimization results. In this section a validation study is carried out for our current analysis and design tools. First, a high speed flight condition of the UH-60A rotor is simulated using time-spectral and time-accurate CFD computation methods. Both are obtained using fully coupled CFD/comprehensive analysis solution for a trimmed rotor at convergence. Results are compared with flight test data. Second, the pitching motion of a NACA 0012 airfoil was simulated. The gradients of the time-averaged drag coefficient with respect to airfoil shape changes were calculated by the adjoint method, based on a time-spectral computation. The gradients are compared with finite difference results. Finally, an application of the adjoint-based design methodology to the problem of steady hovering flight of the UH-60A rotor is shown.

A. CFD Flow Solver: SUmb

A three-dimensional, compressible Navier-Stokes flow solver, SUmb (Stanford University multi-block), has been utilized for all computations in this paper. SUmb is a multi-block structured grid flow solver developed at Stanford University under the sponsorship of the Department of Energy Advanced Strategic Computing (ASC) program. Various turbulence models are implemented to capture the viscous and turbulent properties of the flow: Baldwin-Lomax, Spalart-Allmaras, $k-\omega$, Menter SST, and v^2-f. SUmb is a massively parallel code (in both CPU and memory) using a scalable pre-processor, load balancing, and MPI. It employs multigrid, Runge-Kutta time stepping for the mean flow, and a DD-ADI solution methodology for the turbulence equations. Central difference discretization (second-order in space) with several artificial dissipation options (scalar or matrix), or upwind discretization is available for the spatial discretization. For unsteady time integration, second-/third-order backwards difference formula[25] (BDF) or the time-spectral approach for time-periodic flows can be used. SUmb has been successfully used in many applications, including simulations of launch vehicles, space and re-entry vehicles, jet/turbo engines, subsonic and supersonic aircraft, and helicopter rotors. For the UH-60A rotor validation study, a second-order BDF scheme was used for the time-accurate computation, and a second-order upwind scheme with Roe's flux differencing was used for the inviscid fluxes. The Spalart-Allmaras turbulence model was employed.

B. Time-Spectral Method for Rotor Flow Analysis

Time-spectral analysis of rotor flows has a practical importance when it comes to the prediction of the rotor loads (both airloads and structural loads) because the dominant frequencies of interest are typically limited to two or three multiples of blade numbers. A precise prediction of rotor airloads and structural loads requires the calculation of blade elastic deformations and unsteady control angles obtained from an iterative solution procedure using a CFD/CA coupling method. Thus the capability of the time-spectral method in an aeroelasticity analysis is of great significance for the method to be trusted for the realistic analysis of

rotorcraft. The cost savings of the time-spectral method should also be able to make the coupling process more efficient than that of a time-accurate computation.

The time-spectral method has been well validated for rotor flows in our previous studies.[5–7,22] It has been tested for several of the critical level flight conditions of the UH-60A (high speed, low speed, and dynamic stall cases). The results from the high speed case, counter 8534, are shown here for validation purposes: speed ratio $\mu = 0.368$ (155 kts), vehicle weight coefficient to solidity ratio $C_W/\sigma = 0.0783$, and a longitudinal shaft tilt angle of $\alpha = 7.31°$ (tilt-forward). The predicted rotor thrust level (along the shaft) for this flight is $C_T/\sigma = 0.084$, around 17,500 lb.

This particular flight condition is important for testing design optimization capability because it represents a high advance ratio condition with high vibration. Comprehensive analyses using lifting line and free wake models are not able to accurately capture the advancing blade transonic flow and corresponding structural deflections, while CA coupling with CFD has played a key role in improved section pitching moment and vibration prediction.[26,27] In this case, high fidelity CFD is seen to be a critical tool for accurate rotor design for high speed flight.

1. *CFD/Comprehensive Analysis Coupling*

For validation purposes the time-spectral analysis is coupled to a rotorcraft comprehensive analysis, UMARC (University of Maryland Advanced Rotorcraft Code).[28] During the time-spectral computation/comprehensive analysis coupling, UMARC supplies the structural dynamic model, the free-flight trim model, and the airload sensitivities as required by the iterative delta coupling method. A second-order BDF scheme with dual-time stepping is used for thetime-accurate computation, while a total of 11 time instances are employed for the time-spectral computation. The computational mesh for both methods are shown in Figure 1. A full wake capturing approach is used for the analyses. The resulting sectional force components of normal force, pitching moment, and chord force are plotted in Figures 2, 3, and 4, respectively, and compared with Army/NASA flight test data.[29] Comparison between time-accurate and time-spectral computations shows overall good agreement, and both results match reasonably well with flight test data. A detailed discussion of these results is available in the References.[7]

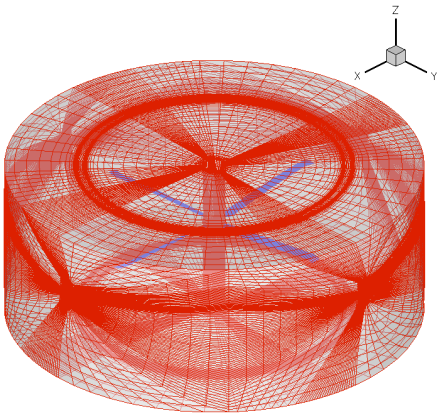

Figure 1. 4-bladed UH-60A mesh(536 blocks with about 17 million nodes).

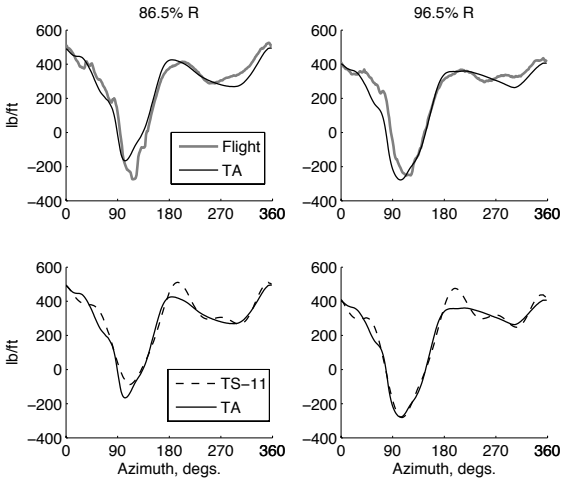

Figure 2. Measured and predicted normal forces for the UH-60A in high speed flight C8534.

2. *Single Blade Analysis*

A complete rotor analysis was employed for the validation study in the previous section that uses a mesh topology of four blades and full wake capturing by the CFD solver. On the other hand, a single-blade CFD analysis coupled with an external free wake model is an efficient alternative, though less accurate.[30] Only the near-field is calculated by CFD (Figure 5), whereas the far-field, which includes the effect of the other blades, is accounted for via the inflow generated by a free wake model and incorporated within the near-blade

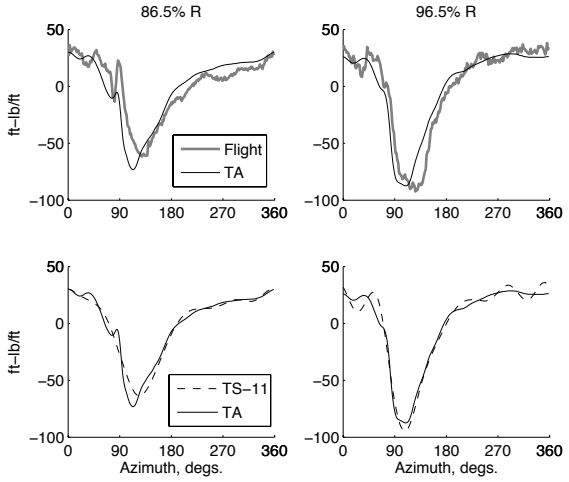

Figure 3. Measured and predicted quarter chord pitching moments for the UH-60A in high speed flight C8534.

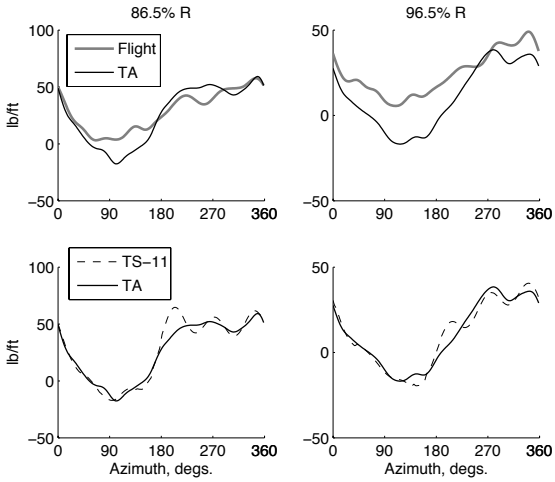

Figure 4. Measured and predicted chord forces for the UH-60A in high speed flight C8534.

CFD domain using the field velocity approach.[30] The computational efficiency obtained by the reduction of the computation domain is considerable and does not substantially deteriorate the accuracy of the solution for these flight conditions. We employ a single blade analysis approach without the wake model in our design optimization study to further simplify the design problem.

The different approaches were tested for high speed Counter 8534 case and showed similar accuracy[5] in the prediction of airloads, as the blade-wake interaction and induced inflow are minimal in this flight condition. This trend is shown in Figures 6, 7, and 8 that the airloads predictions agree reasonably well among the complete rotor analysis, single blade with wake coupling, and single blade analysis without wake coupling. All three analyses use uncoupled, prescribed blade deformations and trim angles from an alternate OVERFLOW/CAMRAD analysis.[26] Once the validity of our design tool is proved in the current paper, its application to a complete 4-bladed rotor analysis with a full wake capturing approach is straightforward as long as enough computational resources can be provided.

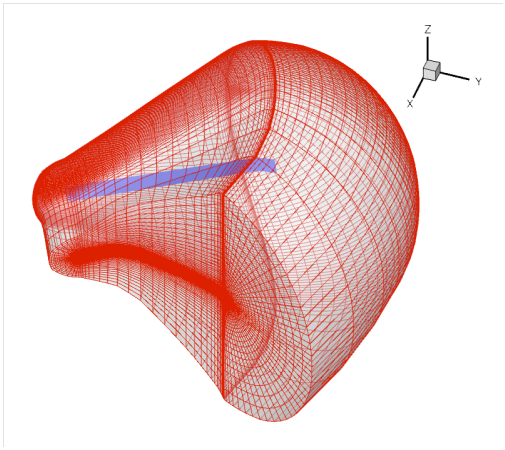

Figure 5. 1-bladed UH-60A mesh (568,816 nodes).

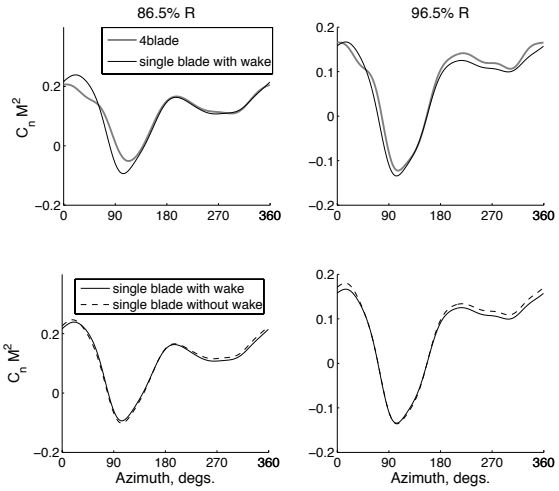

Figure 6. Predicted normal forces for the UH-60A in high speed flight C8534.

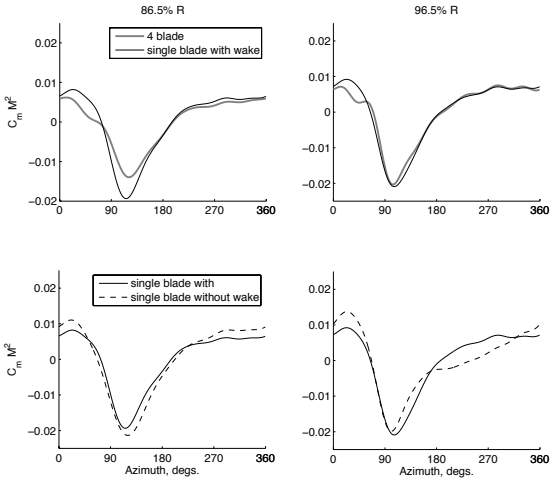

Figure 7. Predicted quarter chord pitching moments for the UH-60A in high speed flight C8534.

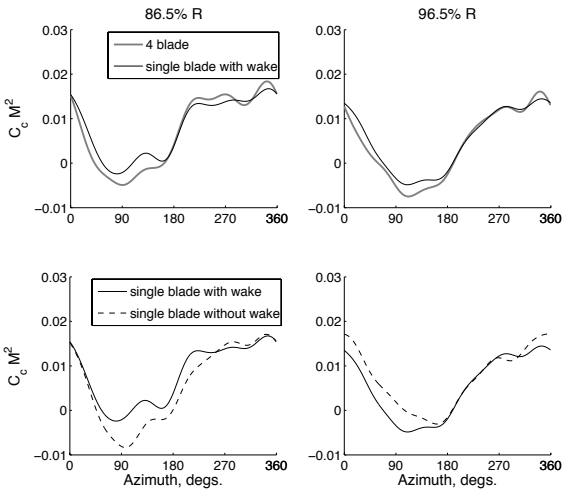

Figure 8. Predicted chord forces for the UH-60A in high speed flight C8534.

C. Validation of Adjoint Solution using Time-Spectral Computation

The pitching motion of a NACA 0012 airfoil was simulated at two inviscid flow conditions, transonic ($M_\infty = 0.8$) and supersonic ($M_\infty = 2.0$). The airfoils were pitched about the quarter chord with a reduced frequency of $k = 0.2$ and with a pitching motion amplitude of $\pm 5^o$. The corresponding angular frequencies were $\omega = 35.43$ and 88.5HZ for the transonic and supersonic flow conditions, respectively. A total of six time instances for the pitching motion period were used for both the flow and discrete adjoint solution. A quasi-three dimensional body-fitted O-mesh with $81 \times 17 \times 9$ grid points were used for all the calculations. A comparison of the transonic and supersonic time-spectral results with a time-accurate computation using second-order BDF and a dual time-stepping approach has shown good agreement.

To assess the accuracy of the resulting discrete adjoint solution, a finite difference method was used to compare the sensitivity of the time-averaged drag coefficient with respect to the amplitude of Hicks-Henne bump functions centered at mesh points on the upper surface of the airfoil. The Hicks-Henne functions are smooth functions that can be used to modify the shape of the airfoil.

The values of the sensitivities of the average drag coefficient over a pitching cycle, $\overline{C_D}$, computed using both the time-spectral adjoint solutions and the method of finite differences are shown in Figure 9. The finite difference results use carefully chosen step sizes to yield accurate derivatives. The agreement between these two approaches gives us confidence that the results of the time-spectral adjoint calculations are correct. Small differences between the two results still exist and are attributed to the fact that the time-spectral adjoint operator we have implemented has neglected some variations of the residual $R^*(u)$ involving the spectral radius computation and the artificial dissipation coefficients.

D. Design Application to Hover

An application of the design method was carried out for a steady hover flight condition of the UH-60A rotor. Since this application was studied in our previous work,[22] only a brief summary is shown here. Although a hovering rotor can be transformed to a steady problem using one time instance, we simulated it as periodic and unsteady in order to test the time-spectral design method. The objective is the minimization of the torque to thrust ratio. A single blade Euler analysis is employed for simplification of the problem. A free wake is included as the wake effects in hover flight can not be neglected. A total of three time instances are used for both the flow and adjoint solvers.

An advantage of designing for the hover condition is that constraint handling is more straightforward as trim related parameters do not need to be included. We employed a nonlinear multi-dimensional conjugate gradient method for an optimization algorithm. Since the conjugate gradient method is not able to impose constraints, a thrust constraint is integrated into the objective function. Using the nondimensionalized

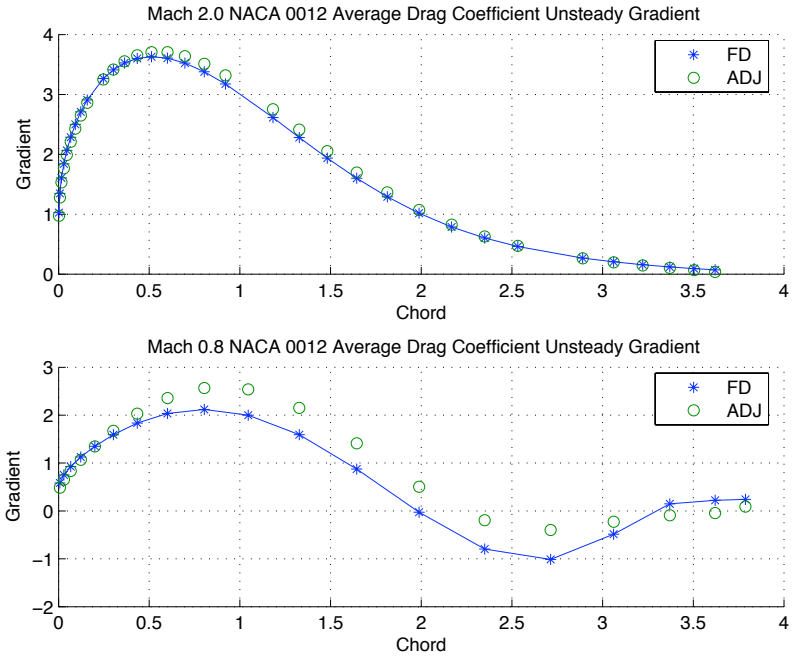

Figure 9. Comparison of sensitivity derivatives $\frac{\partial \overline{C_D}}{\partial b_i}$ using discrete adjoint solution (ADJ) and finite differences (FD) for the supersonic (top) and transonic (bottom) test cases.

coefficients of torque, C_Q, and thrust, C_T, the mathematical formulation of the objective function is

$$I = C_Q/C_T \ , \tag{15}$$

Blade shape modifications were obtained by imposing smooth Hicks-Henne bump functions on the surface of the airfoils along the span, and the corresponding new meshes were obtained in a fast manner using a mesh warping routine without the need for complete mesh regeneration. As the gradient-based optimization algorithm performs best with a smooth design space, the shape changes described by the amplitude of the bump functions are limited to small amounts, with the assumption that minor variations in shape result in a smooth design space. A total of nine sections along the span were selected, with even distribution on the blade mid-span sections and tighter distribution on the blade inboard sections and swept tip region. Perturbations were applied at each section at ten locations on the airfoil surface. The maximum bump amplitudes were scaled to the local airfoil thickness. A total of 90 design variables (amplitudes of the bump functions) were introduced. Inclusion of more design variables do not significantly affect the results.

Throughout the design iterations, constant prescribed aeroelastic deformations[26] were maintained using the initial values. While the structural properties would not be expected to change significantly due to small airfoil shape changes, any redistribution of the span loading or changes in sectional pitching moments might affect the elastic deformation. This CFD/CSD coupling influence was not considered in the design.

Optimized results were obtained after 19 design iterations. A 12% torque reduction was achieved with a 7% thrust increase. These values come as a surprise, considering the small variations in the airfoil shapes (mainly camber and thickness changes), but this fact implies that aerodynamic loads are sensitive to even small changes in the airfoil shapes or span load distribution. As the shape changes are limited to the small variations, the direct comparison of shapes between the baseline and the optimized blade is not obvious. Changes in the pressure distribution on the blade upper and lower surfaces are shown in Figure 10. It can be noted that pressure around the tip area becomes lower and contributes to reducing the pressure drag.

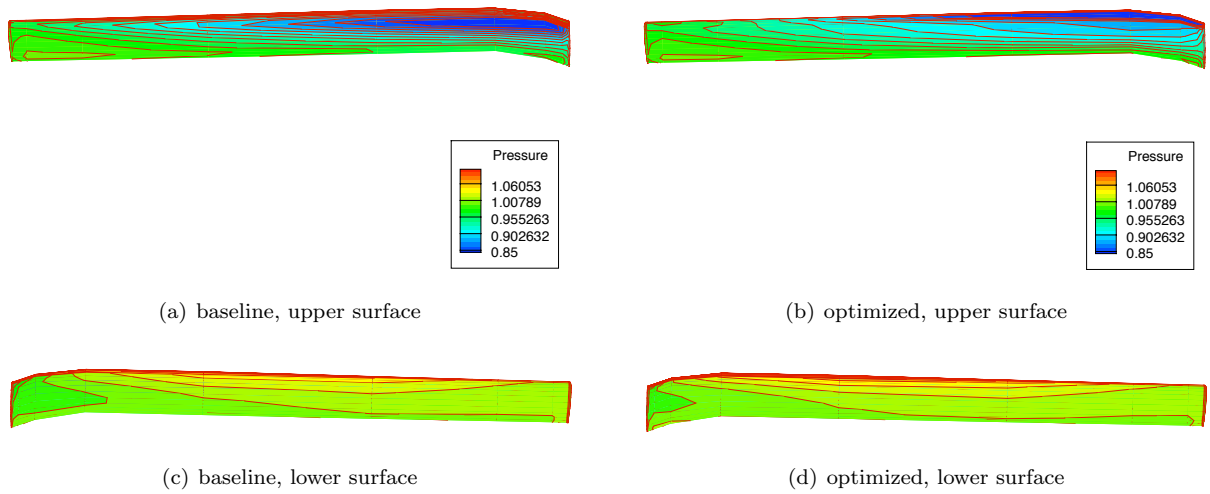

(a) baseline, upper surface

(b) optimized, upper surface

(c) baseline, lower surface

(d) optimized, lower surface

Figure 10. Comparison of the surface pressure contours between the baseline and the optimized rotor blade in hover.

V. RESULTS

The current work is the extension and application of the design methodology from steady hover to unsteady, periodic forward flight condition. Planform shape changes are considered in addition to sectional airfoil shape and twist changes. A gradient-based optimization algorithm which can impose bounds on the design variables and constraints on the objective function is employed.

A. Design Problem Specification

The time-spectral method has been implemented in a viscous flow solver which has various turbulence models available. It is well validated for the computation of rotor flows using a complete rotor disk analysis with full wake capturing. However, the discrete adjoint formulation is currently only implemented for inviscid flow, and, thus, our design optimization scope is limited to an Euler computation. High speed flight Counter 8534 for UH-60A is chosen as the test case. Viscous effects for these flight conditions are not severe, and use of an Euler computation is acceptable.[27] A single blade analysis without wake coupling is employed. A total of 9 time instances are used for the time-spectral and adjoint computations. The choice of the number of time instances and single blade analysis approach was made based on the previous study,[5,7] and to maximize the computational efficiency without losing the desired accuracy. The lack of wake coupling is reasonable given the large forward shaft tilt and high speed conditions.

A minimization of rotor torque is pursued as an objective of the optimization problem. A constant or higher thrust level than the initial value and non-increasing drag force are enforced as non-linear constraints. One of the difficulties associated with design at forward flight conditions is the imposition of helicopter steady level flight trim conditions as realistic constraints. In high speed flight the rolling moment constraint is particularly difficult to satisfy due to the large differences in dynamic pressure on the advancing and retreating blades. Trim requires an extended optimization process via CFD/CA coupling iterations at each design step which provides a new set of control angles and elastic deformations from the previous design step. Although this CFD/CA coupling procedure for trim has already been carried out with the time-spectral method,[6,7] its direct integration into the design procedure has not been tested, the increase in computational time is prohibitive, and the adjoint solution procedure with the structural analysis code is not straightforward. Also, changes in the blade shape (planform) affects the structural properties of the blade. Variations in the elastic and torsional stiffnesses as well as changes in the location of the elastic axis will certainly change the elastic blade deformation. However, calculating the structural properties of a new rotor blade is not simple and is beyond the scope of this aerodynamic design optimization work. Therefore, a true trim condition as a realistic constraint is not considered within our design scope. Its simplified form of a thrust and drag-force constraint is imposed in the current problem. However, in order to take into account some effects of the controls input, blade deformation, and elastic torsion for the c8534 case, blade motions

from an OVERFLOW/CAMRAD analysis[26] are imposed constantly throughout the entire design iterations. It is not reasonable to neglect these effects entirely for high aspect ratio, rotating blades.

Design variables are chosen to change the planform shape of the outboard part of the blade and the airfoil sections along the span. The twist distribution of the baseline blade is also allowed to vary. The leading edge locations and chord lengths vary at three radial locations: 85, 95, and 100% R. The twist distribution is modified at 10 radial locations along the span. The locations of the twist changes are largely in the tip area where the blade tip typically experiences the most dynamic and variable flow phenomena such as blade-wake interaction, transonic flow with shocks, and dynamic stall. The mid-span area has only two twist change locations. Airfoil shapes at 9 radial locations along the span are modified by applying Hicks-Henne bump functions. At each section, 10 bump functions are applied with maximum bump locations fixed at given positions. The amplitudes of the bumps are allowed to vary as design variables. The airfoil shapes at the sections between the design locations are linearly interpolated. Thus, a total of 106 design variables are used to change the planform and airfoil sections of the blade. The bounds of each design variable are carefully chosen such that the mesh generator can handle the geometry variation and, at the same time, the variation is large enough for the optimizer to explore a large area of the design space. The lower and upper bounds of the design variables are shown in Table 1. Negative and positive variation is added to the baseline values. A more robust grid generator than currently used and/or spanwise gradient smoothing is required in order to allow for additional design freedom of the outboard planform shape so that a BERP-like shape could be explored.

baseline variable	design variables	lower bound	upper bound
x_1	leading edge location at 85% R	$x_1 - 0.15$	$x_1 + 0.15$
x_2	leading edge location at 95% R	$x_2 - 0.2$	$x_2 + 0.2$
x_3	leading edge location at R	$x_3 - 0.5$	$x_3 + 0.5$
x_4	chord length at 85% R	0.7 x_4	1.3 x_4
x_5	chord length at 95% R	0.7 x_5	1.3 x_5
x_6	chord length at R	0.7 x_6	1.3 x_6
x_7	twist (^{o}) at 13% R	$x_7 - 0.2$	$x_7 + 0.2$
x_8	twist (^{o}) at 17% R	$x_8 - 0.2$	$x_8 + 0.2$
x_9	twist (^{o}) at 19% R	$x_9 - 0.2$	$x_9 + 0.2$
x_{10}	twist (^{o}) at 26% R	$x_{10} - 3.4$	$x_{10} + 3.4$
x_{11}	twist (^{o}) at 42% R	$x_{11} - 7.84$	$x_{11} + 7.84$
x_{12}	twist (^{o}) at 65% R	$x_{12} - 7.7$	$x_{12} + 7.7$
x_{13}	twist (^{o}) at 85% R	$x_{13} - 7.8$	$x_{13} + 7.8$
x_{14}	twist (^{o}) at 95% R	$x_{14} - 4.9$	$x_{14} + 4.9$
x_{15}	twist (^{o}) at 98% R	$x_{15} - 1.8$	$x_{15} + 1.8$
x_{16}	twist (^{o}) at 99.9% R	$x_{16} - 1.0$	$x_{16} + 1.0$
$x_{17} \sim x_{106}$	amplitude of bump function	-0.8% of chord length	0.8% of chord length

Table 1. Design variables and their lower and upper bounds

B. Optimization Procedure and Results

We use a gradient-based optimization tool, NPSOL,[31] that is a sequential quadratic programming (SQP)-based method. It is a software package for solving constrained optimization problems. It represents the objective as a quadratic approximation to the Lagrangian and employs a dense SQP algorithm to minimize a quadratic model of the problem.[32] The algorithm is especially effective for nonlinear programming problems whose functions and gradients are expensive to evaluate. It is intended for problems with up to a few hundred constraints and variables, with a main limitation being the amount of memory available for the analysis. Thus, the algorithm is ideal for our current problem type which includes hundreds of design variables and produces gradients of the objective and constraints with respect to each design variable.

The entire design optimization procedure is summarized in Figure 11. With given design variables, the airfoil shape at each section is modified by applying the bump functions to the airfoil surface, and a new blade with planform and twist changes is automatically generated by a mesh generator. Time-spectral flow solution computations are obtained to calculate the values of the objective function and constraints. The resulting flow field state vectors are input to the discrete adjoint solver to compute the adjoint solutions. Sensitivity information is calculated in a fast manner via simple vector operations using the adjoint variables. The values of the objective, constraints, and their sensitivity information are provided to the optimizer, and a new set of design variables corresponding to a design candidate in the search direction is returned at each design iteration. This procedure is repeated for several design iterations until the specified convergence criteria is met.

The initial configuration (Figure 12) used as the starting point for the optimization was not exactly the same as the c8534 baseline of the UH-60A used for the time-spectral validation shown earlier. Variation of the initial configuration from the baseline, however, allows us to see whether the optimized configuration approaches the original baseline that was designed by industry through experimental tests and analysis, and if the optimizer can come up with a new design which shows better performance than the baseline.

After about 38 design iterations, we obtained the optimized configuration which is shown in Figure 13. When compared with the initial configuration, the optimized results shows a performance improvement with a decrease in torque (by more than 20%) while maintaining thrust (increase of less than 1%). Even when compared with the baseline UH-60A, these results amount to an increase in thrust of almost 7% and a small decrease in torque of about 2%. As a direct comparison between the optimized and the baseline is more meaningful, the comparisons shown here will be mostly with the original baseline configuration of the UH-60A. However the sectional airload comparisons are shown among the initial configuration, the baseline, and the optimized. It should be noted that if we want a relative improvement in performance from the baseline, then our initial starting point should be the original baseline, but that will be just another application example of our design methodology and is left for future work.

A detailed comparison of the leading edge locations and the chord lengths is shown in Figures 14 and 15 for the baseline and optimized. The optimized configuration shows a different tip shape from the baseline, and the variation in the chord length is more noticeable than the small changes in the leading edge location. Difference in twist between the baseline and optimized is shown in Figure 16. It is shown that the optimized result added more positive twist around the root and tip area. Note, however, that the optimized configuration produces higher thrust. The airfoil shape changes through bump function are small compared to the planform shape changes.

Changes in the sectional normal force and chord force coefficients are shown in Figures 17 and 18. The flow direction is from $\psi = 180$ to 0^o, with the advancing and retreating blades at 90 and 270 ^{o}, respectively. Sectional normal forces along the inboard span up to 55% R do not appear to change much for all azimuthal locations, but from mid-span up to 86.5% of the span, the increase of the sectional normal force is shown mainly on the advancing side. However, the blade tip area experiences an increase in sectional normal force at all azimuthal angles. The largest increase in lift is observed in the first and third quadrants of the domain on the front and rear of the rotor disk. In general this is where the rotor generates its thrust forces at high speed conditions, while the sides of the rotor disk (advancing and retreating blades) fight to maintain roll trim. Similarly, sectional chord forces, which contribute to torque, are increased in the blade tip area at all azimuthal positions and a slight increase is also shown in the root area on the advancing side. It should be noted that due to the chord change on the outboard span, comparison of section coefficients is not entirely useful as a direct measure of thrust and torque, which would be more clearly seen in polar plots of $c\, C_n M^2$ and $c\, C_c M^2$.

Figures 19 – 22 compare the airfoil section shapes and sectional pressure coefficients distributions between the baseline and optimized at $\psi = 80^o$ (second time instance) at four radial locations, 81.7, 91.8, 96.7 and 99.0 % R, respectively. The thinner leading edge, twist increase, and reduced chord are observed in the optimized configuration. On the most outboard sections, the twist has increased but the minimum pressure on the airfoil has not changed due to the shape optimization. The shocks at these locations have move considerably aft with a relatively flat rooftop distribution. Although the original airfoils have sharp trailing edges, which is also a constraint of the grid generator, the optimizer has attempted to increase the trailing edge thicknesses.

The uneven increase in sectional forces around the rotor disk leads to an overall increase in lift on the advancing side and a decrease on the retreating side. This fact adversely affects the moment balance of the

rotor, and causes an undesirable rolling moment, which deteriorates the trim condition. However zeroing of the rolling moment is not included as a constraint in our optimization, and it is evident that the optimizer is exploiting this fact to drive to a lower torque at higher or constant thrust level. On the other hand, a secondary constraint of non-increasing drag force is well satisfied. This result emphasizes, again, the importance of realistic constraints for a viable rotor design optimization, and, at the same time, reminds us of the difficulty in imposing the vehicle trim conditions. Without CFD coupling with structural and comprehensive analyses, which provide structural dynamics, elastic deformation, and control angle inputs for the new trim state, a force and moment equilibrium is overly simplistic.

Therefore, multidisciplinary design optimization for the current problem is planned for future work, and the overall design procedure is shown in Figure 23. As an alternative to tight coupling between aerodynamic analysis and rotorcraft comprehensive analysis, a loose iterative coupling between aerodynamic optimization and comprehensive analysis based trim optimization will be considered. If the force and moment balances are enforced in the aerodynamic optimization, the differences in control angles and elastic responses at each iteration will become smaller, reaching global convergence for the multidisciplinary optimization.

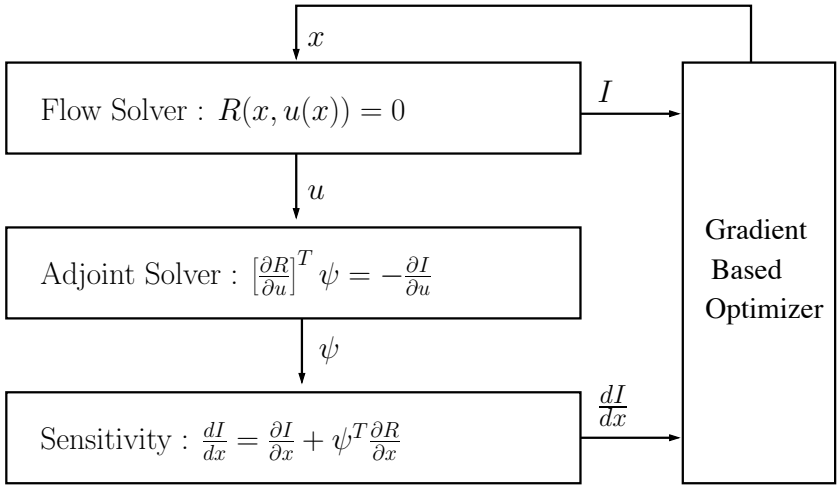

Figure 11. Design optimization procedure.

Figure 12. Baseline planform shape.

Figure 13. Optimized planform shape.

VI. CONCLUSIONS

An efficient and accurate analysis and design optimization methodology using time-spectral and discrete adjoint-based methods has been developed. The methodology is particularly attractive for periodic unsteady flows, such as helicopter rotors in forward flight. The time-spectral method is a Fourier collocation method applied to the temporal discretization of the governing equations of periodic, unsteady problems. The introduction of the Fourier spectral derivative in the time-spectral method renders the governing equations to be steady-state in the time domain. This enables the adjoint method to be employed as a steady formulation for the unsteady problem. A high speed flight condition (Counter 8534) for the UH-60A Black Hawk helicopter was chosen as a test problem. Validation of the time-spectral CFD analysis was shown in comparison with time-accurate analysis and flight test data. The design methodology was employed to optimize the planform shape and airfoil sections in order to minimize the rotor torque with non-linear thrust and drag force constraints. Variation from the UH-60A baseline was employed as an initial point of optimization. The

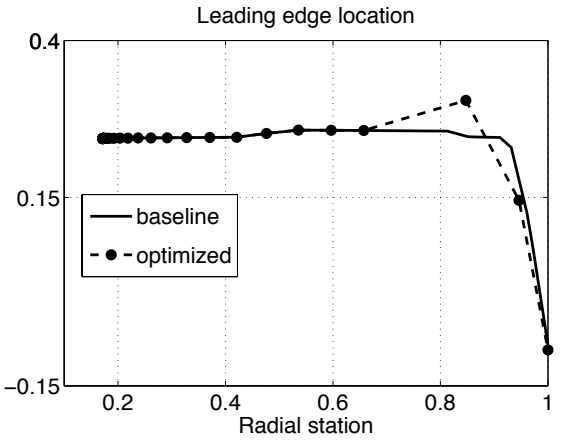

Figure 14. Comparison of leading edge location.

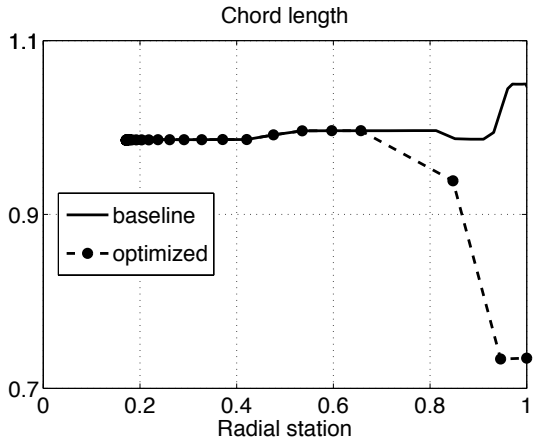

Figure 15. Comparison of chord length.

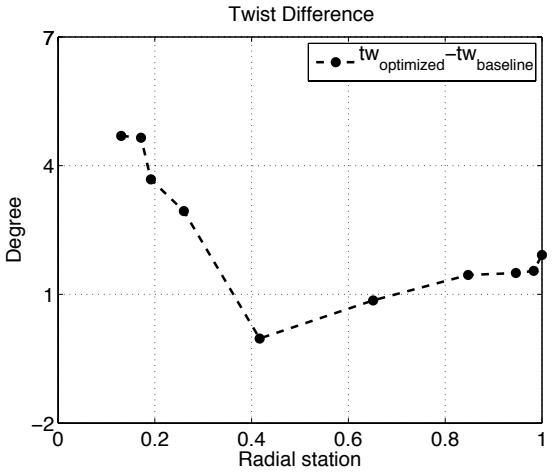

Figure 16. Difference in twist between the baseline and optimized along the span.

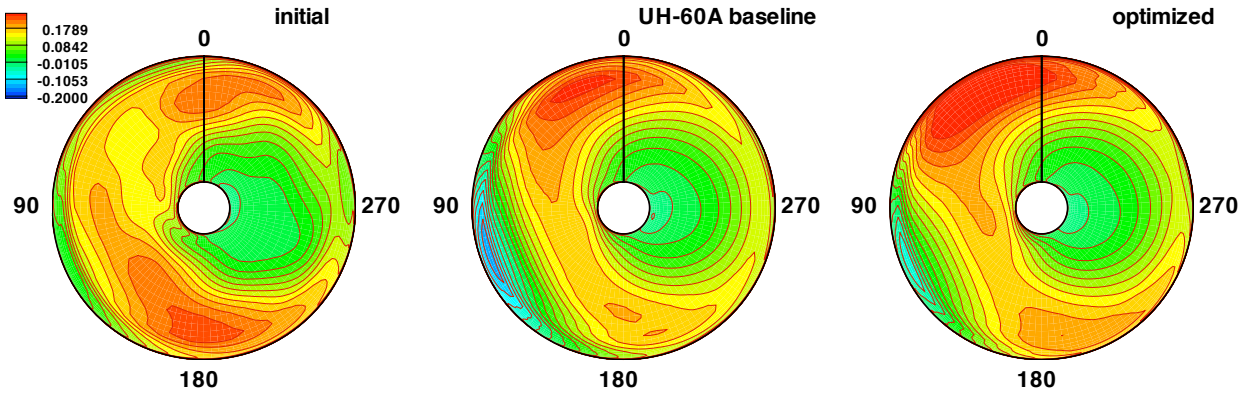

Figure 17. $C_n M^2$ plot comparison between baseline and optimized. 0 deg. aft.

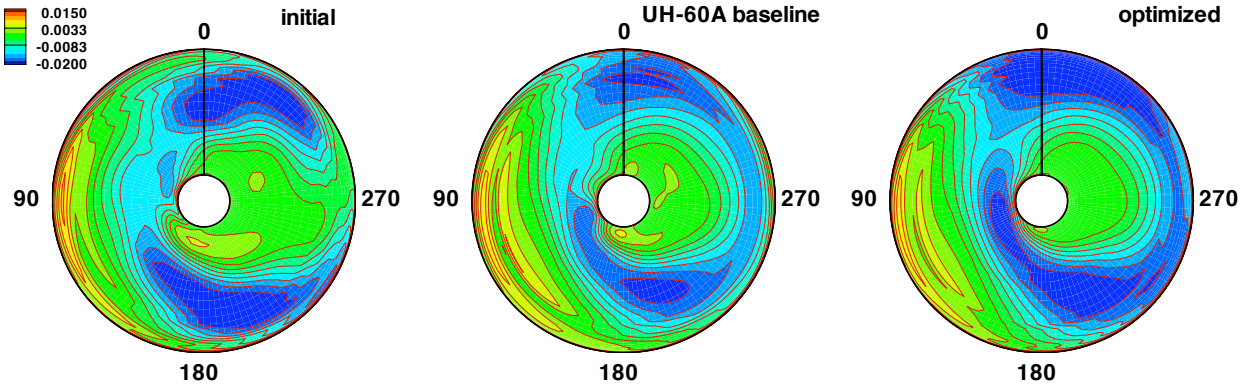

Figure 18. $C_c M^2$ **plot comparison between baseline and optimized. 0 deg. aft.**

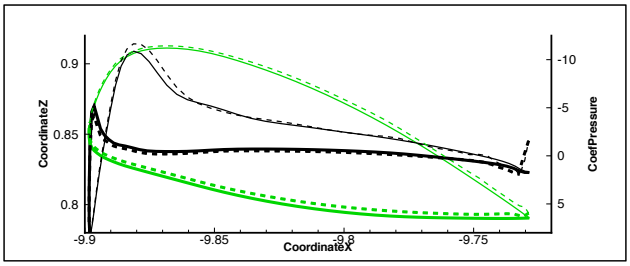

Figure 19. Airfoil sections and Cp plots at radial location of 81.7% R, and $\psi = 80^o$ (solid:baseline and dashed:optimized, lower surface bold).

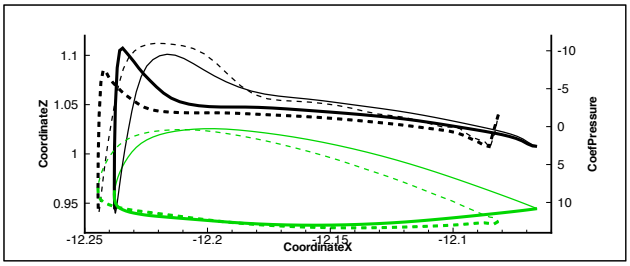

Figure 20. Airfoil sections and Cp plots at radial location of 91.8% R, and $\psi = 80^o$ (solid:baseline and dashed:optimized, lower surface bold).

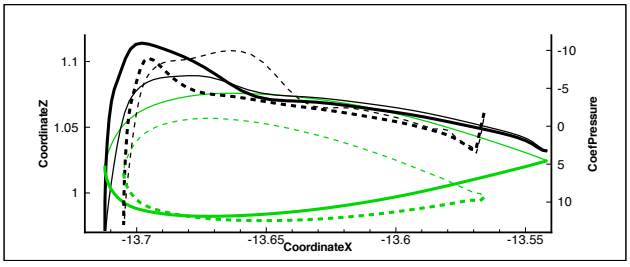

Figure 21. Airfoil sections and Cp plots at radial location of 96.7% R, and $\psi = 80^o$ (solid:baseline and dashed:optimized, lower surface bold).

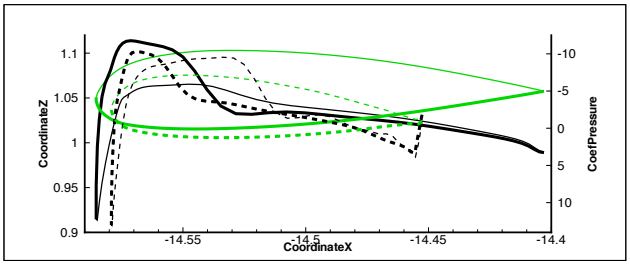

Figure 22. Airfoil sections and Cp plots at radial location of 99.0% R, and $\psi = 80^o$ (solid:baseline and dashed:optimized, lower surface bold).

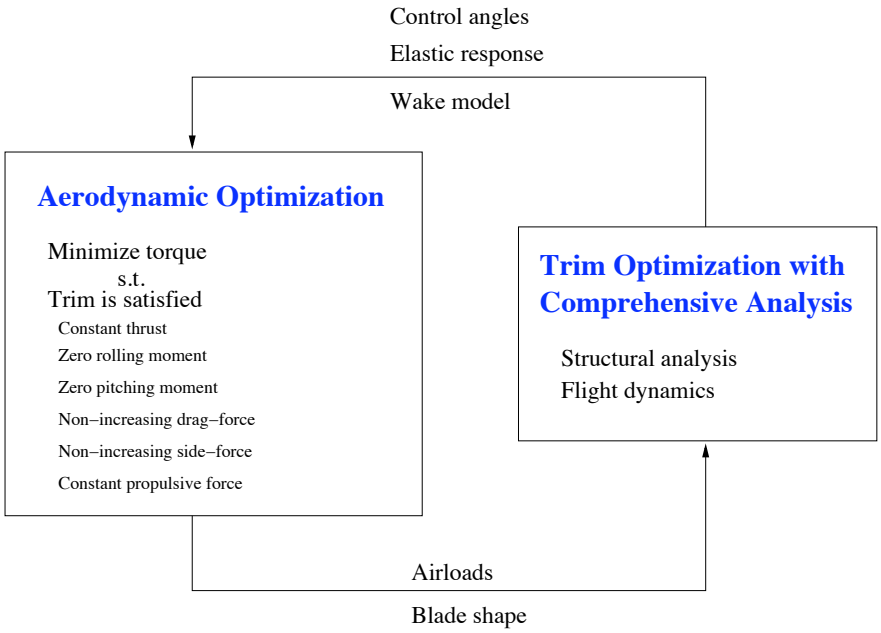

Figure 23. Multidisciplinary Design optimization procedure.

optimized result showed a performance improvement over the initial configuration - a similar thrust level and a decrease in the torque by more than 20%. In comparison with the original baseline, it demonstrates a 7% increase in thrust and a 2% decrease in torque. However without realistic constraints for the trim condition, which would require complex multidisciplinary CFD/CSD and comprehensive analysis iterative coupling, the result shows an undesirable rolling moment due to uneven increase in the lift on the rotor disk. Based on our study in this paper, following key conclusions are drawn:

1. The time-spectral methodology allows an unsteady periodic problem to be transformed into a steady-state formulation, enabling the use of steady-state adjoint-based design methods.

2. The time-spectral and adjoint-based design methodology was successfully applied to the realistic unsteady problem of helicopter rotor analysis and design in forward flight using high fidelity, high performance computational fluid dynamics.

3. More realistic multidisciplinary trim and structural constraints need to be included for a viable design. This requires iterative coupling of the aerodynamic design procedure with a computational structural dynamics and rotorcraft comprehensive analysis capability, as was demonstrated for analysis validation.

VII. ACKNOWLEDGEMENT

This work has been carried out under the support of the Aeroflightdynamics Directorate (AFDD) at Ames Research Center, under contract NNA06CB11G. We gratefully acknowledge the support of Tom Maier and Roger Strawn for supplying us with experimental data and the technical advice necessary to complete this study. We also thank the University of Maryland for providing us with a mesh generator.

References

[1]Canuto, C., Hussaini, M. Y., Quarteroni, A., and Zang, T. A. Jr., "Spectral Methods in Fluid Dynamics," *Springer,* 1998.

[2]Hesthaven, J., Gottlieb, S., and Gottlieb, D., "Spectral Methods for Time-Dependent Problems," *Cambridge Monographs on Applied and Computational Mathematics,* 2007.

[3]Gopinath, A., and Jameson, A., "Time spectral method for periodic unsteady computations over two- and three- dimensional bodies," *AIAA Paper 05-1220*, Reno, NV, Jan. 2005.

[4]Van der Weide, E., Gopinath, A., and Jameson, A., "Turbomachinery applications with the time spectral method," *AIAA Paper 05-4905*, Toronto, Canada, Jun. 2005.

[5]Choi, S., Alonso, J. J., Van der Weide, E., and Sitaraman, J., "Validation Study of Aerodynamic Analysis Tools for Design Optimization of Helicopter Rotors," *AIAA Paper 07-3929*, Miami FL., June 2007.

[6]Choi, S., and Datta, A., "Time-Spectral Method for the CFD Prediction of Main Rotor Vibratory Loads," *5th International Conference on CFD*, Seoul Korea, July 2008.

[7]Choi, S., and Datta, A., "CFD Prediction of Rotor Loads using Time-Spectral Method and Exact Fluid-Structure Interface" *26th AIAA Applied Aerodynamics conference, AIAA paper 08-7325*, Honolulu Hawaii, Aug. 2008.

[8]Thomas, J. P., Dowell, E. H., and Hall, K. C., "Modeling Three-dimensional Inviscid Transonic Limit Cycle Oscillation using a Harmonic Balance Approach," *ASME International Mechanical Enginnering Conference and Exposition*,New Orleans, 2002.

[9]Kumar, M., and Murthy, V., "Efficient Rotor Flow Calculation Using Multiblade Coordinate Transformed CFD in Frequency Domain," *AIAA-2008-408, 46th AIAA Aerospace Sciences Meeting and Exhibit*, Reno, Nevada, Jan. 7-10, 2008.

[10]Ekici, K., Hall, K., and Dowell, E., "Computationally Fast Harmonic Balance Methods for Unsteady Aerodynamic Predictions of Helicopter Rotors," *AIAA-2008-1439, 46th AIAA Aerospace Sciences Meeting and Exhibit*, Reno, Nevada, 2008.

[11]McMullen, M. S., and Jameson, A., "The Computational Efficiency of Non-Linear Frequency Domain Methods," *Journal of Computational Physics,* Vol. 212, Issuse 2, pp.637–661, March 2006.

[12]Nadarajah, S., McMullen, M., and Jameson, A., "Aeroelastic Solutions using the Time Accurate and Non-Linear Frequency Domain Methods," *AIAA Paper 2006-0445, 44th Aerospace Sciences Meeting and Exhibit,* January 9 - 12, 2006, Reno, Nevada.

[13]Reuther, J. J., Jameson, A., Alonso, J. J., Rimlinger, M., and Saunders, D., "Constrained multipoint aerodynamic shape optimization using an adjoint forumlation and parallel computers: Part I & II," *Journal of Aircraft,* 36(1):51-74,1999

[14]Jameson, A., "Aerodynamic design via control theory ," *Journal of Scientific Computing, 3:233-260*,1988

[15]Martins, J. R. R. A., "A Coupled-Adjoint Method for High-Fidelity Aero-Structural Optimization," *Ph.D dissertation*, Department of Aeronautics and Astrounautics, Stanford University, Stanford, CA, Oct. 2002.

[16]Kim, S., Alonso, J. J., and Jameson, A., "A gradient accuracy study for the adjoint-based Navier-Stokes design method," *AIAA Paper 99-0299*, Reno, Jan. 1999.

[17]Leoviriyakit, K., and Jameson, A., "Aero-structural wing planform optimization," *AIAA 42nd Aerospace Science Meetings & Exhibit,*Reno, NV, Jan. 2004.

[18]Mani, K., Mavriplis, D. J., "An Unsteady Discrete Adjoint Formulation for Two-Dimensional Flow Problems with Deforming Meshes," *AIAA 45th Aerospace Science Meetings & Exhibit,*Reno, NV, Jan. 2007.

[19]Palaniappan, K., Sahu, P., Alonso, J. J., and Jameon, A. "Active flutter control using an adjoint method," *AIAA Paper 2006-0844*, Reno, NV, Jan. 2006.

[20]Nadarahah, S., McMullen, M., and Jameson, A., "Optimal control of unsteady flows using time accurate and non-linear frequency domain methods," *AIAA Paper 2003-3875*, Orlando, FL, Jun. 2003.

[21]Kachra, Farid, and Nadarajah, Siva, "Aeroelastic Solutions using the Time Accurate and Non-Linear Frequency Domain Methods", *AIAA Paper 2006-0445, 44th Aerospace Sciences Meeting and Exhibit,* January 9 - 12, 2006, Reno, Nevada.

[22]Choi, S., Lee, K., Alonso, J. J., and Datta, A., "Study on Time-Spectral and Adjoint-Based Design Optimization of Helicopter Rotors," *AHS Specialist's Conference on Aeromechanics*, San Francisco CA., Jan. 2008.

[23]Le Pape, A., and Beaumier, P., "Numerical Optimization of Helicopter Rotor Aerodynamic Performance in Hover," *Aerospace Science and Technology,* , Volume 9, Issue 3, pp. 191–20, April 2005.

[24]Tarzanin, F., and Young, D., "Boeing Rotorcraft Experience with Rotor Design and Optimization," *AIAA-1998-4733, AIAA/USAF/NASA/ISSMO 7th Symposium on Multidisciplinary Analysis and Optimization*, St. Louis, MO, Sep. 2–4.

[25]Jameson, A., "Time dependent calculations using multigrid, with application to unsteady flows past airfoils and wings," *AIAA Journal, 91-1956,* June 1998.

[26]Potsdam, M., Yeo, H. and Johnson, W., "Rotor Airloads Prediction Using Loose Aerodynamic/Structural Coupling," *Journal of Aircraft,* Vol. 43 (3), May–June 2006, pp. 732–742.

[27]Datta, A., and Chopra, I., "Validation of Structural and Aerodynamic Modeling using UH-60A Airloads Program Data," *Journal of the American Helicopter Society*, Vol. 51, (1), January 2006, pp. 43–58.

[28]Datta, A., and Chopra, I., "Validation and Understanding of UH-60A Vibratory Loads in Steady Level Flight," *Journal of the American Helicopter Society*, Vol. 49, No. 3, July 2004, pp 271-287.

[29]Kufeld, R. M., Balough, D. L., Cross, J. L., Studebaker, K. F., Jennison, C. D., and Bousman, W. G., "Flight Testing of the UH-60A Airloads Aircraft," *AHS 50th Annual Forum*, Washington, DC, May 1994.

[30]Sitaraman, J. and Baeder, J., "Field Velocity Approach and Geometric Conservation Law for Unsteady Flow Simulations," *AIAA Journal*, Vol. 44, (9), September 2006, pp. 2084–2094.

[31]Gill, P. E., Murray, W., Saunders, M. A., Wright, M. H., "User's Guide for NPSOL 5.0: A Fortran Package for Nonlinear Programming," *Technical Report SOL 86-1.*, 1998

[32]Gill, P. E., Murray, W., Saunders, M. A., Wright, M. H., "Some theoretical properties of an augmented Lagrangian merit function," *Advances in Optimization and Parallel Computing,* pp. 101–128, P. M. Pardalos, ed., North Holland, 1992